IJIE

INTERNATIONAL JOURNAL OF INTEGRATED ENGINEERING
ISSN: 2229-838X e-ISSN: 2600-7916

Vol. 18 No. 4 (2026) 217-237
https://publisher.uthm.edu.my/ojs/index.php/ijie

Scour Depth Prediction Around a Circular Pier via ANN, SVM, KNN, and RF

Md. Ashraful Islam[1], Md. Mukdiul Islam[1], Md. Samiun Basir[1], Md. Bashirul Islam[2]*

[1] *Department of Water Resources Engineering, Chittagong University of Engineering & Technology, Chattogram, 4349, BANGLADESH*
[2] *Institute of River, Harbor, and Environmental Science, Chittagong University of Engineering & Technology, Chattogram, 4349, BANGLADESH*

*Corresponding Author: bashirul@cuet.ac.bd
DOI: https://doi.org/10.30880/ijie.2026.18.04.015

Article Info

Received: 13 November 2025
Accepted: 9 June 2026
Available online: 20 July 2026

Keywords

Bridge pier, scour depth prediction, machine learning, empirical models, sensitivity evaluation

Abstract

Ensuring bridge safety is vital to prevent major economic and societal impacts. Scour at bridge piers represents a major risk and is determined by factors such as approach flow depth, pier diameter, critical flow velocity, sediment properties, and pier shape. While several empirical equations have been proposed to predict scour depth under clear-water and live-bed conditions, they often show limited accuracy due to their basis in controlled laboratory experiments, narrow data ranges, and inability to capture nonlinear effects. To overcome these issues, this study utilizes machine learning models—including artificial neural networks (ANNs), support vector machines (SVMs), K-nearest neighbors (KNNs), and random forests (RFs)—to estimate normalized scour depth around single circular piers. Model performance is compared to conventional empirical equations using 544 laboratory observations split into training, validation, and testing sets. Accuracy is measured using metrics such as root mean square error (RMSE), mean absolute error (MAE), coefficient of determination (R^2), and Nash–Sutcliffe efficiency (NSE). Visualization methods illustrate the agreement between ML predictions and traditional estimates. Sensitivity analysis shows the pier width–to–flow depth ratio (b/y) as the most critical parameter for predicting normalized scour depth (ds/y). KNN achieves the best results (RMSE = 0.0058, MAE = 0.0943, R^2 = 0.894, and NSE = 0.891). Overall, the findings demonstrate that ML-based approaches can improve scour depth predictions, supporting better bridge design and reducing failure risks from scour.

1. Introduction

Bridge piers are vital to the structural integrity of bridges; however, their stability is threatened by scour, which refers to the erosion of surrounding sediment resulting from the movement of flowing water. This phenomenon compromises the strength and stability of piers, thereby endangering bridge safety. Scour has been identified as a major contributor to bridge failures in numerous studies [1, 2]. Such failures lead to significant economic consequences, including direct expenses for repair or replacement and indirect losses due to transportation disruptions [3]. The drive to minimize these potential damages has led to increased focus on understanding the scour mechanism and developing more reliable methods and equations for scour prediction. When scour depth is underestimated, it may result in bridge collapse, whereas overestimation can cause excessive construction costs [4, 5]. Therefore, precise estimation of scour depth is essential for ensuring safe bridge design and maintenance. Reliable prediction or estimation is crucial for preventing collapse and safeguarding infrastructure.

Traditional scour depth prediction methods generally rely on empirical equations or physical models, which often fail to fully reflect the complex interdependencies between pier geometry, sediment movement, and flow conditions. Conversely, machine learning (ML) offers an effective alternative for scour depth estimation [6]. ML approaches are capable of modeling intricate associations among the numerous variables that influence scour, including water depth, sediment properties, pier configuration, and flow velocity. Compared with conventional techniques, data-driven models often yield more precise and robust predictions [7].

Numerous studies worldwide have explored scour depth estimation using various ML algorithms. For instance, Bateni et al. [8] proposed an approach to forecast scour depth under both time-dependent and equilibrium flow conditions around a pier, employing adaptive neuro-fuzzy inference systems (ANFIS) and artificial neural networks (ANN). Two ANN variants were tested: a radial basis network integrated with an orthogonal least-squares algorithm (RBF/OLS) and a multilayer perceptron trained via a back-propagation algorithm (MLP/BP). Experimental results indicated that the MLP/BP approach surpassed both ANFIS and RBF/OLS in predictive accuracy, with pier diameter identified as the dominant factor for equilibrium scour depth. Choudhary et al. [4] applied gene expression programming (GEP) and an adaptive network-based fuzzy inference system (ANFIS) to develop a predictive model for scour depth at bridge piers. Models were created for both clear-water and live-bed scour scenarios, with ANFIS showing the highest predictive accuracy in both. Eini et al. [9] implemented three hybrid ML strategies: combining red fox optimization (RFO) with XGBoost, particle swarm optimization (PSO) with XGBoost, and relativistic particle swarm optimization (RPSO) with XGBoost. Among these, RPSO-XGBoost achieved the best performance in ranking variable importance. The study also applied the SHapley Additive exPlanations (SHAP) method to evaluate the relative contribution of each factor. Hassan & Jalal [10] developed a novel formula for estimating localized scour depth near a pier using GEP. Their GEP results were compared with a nonlinear regression (NLR) model, and findings showed that GEP outperformed NLR, producing concise mathematical expressions. Kumar et al. [11] used GEP and ANFIS to model the local scour depth at bridge piers and incorporated a temporal dimension by analyzing 500 datasets, with 80% allocated to training and 20% to testing. Their GEP model, cross-validated with ANFIS and empirical equations, achieved R^2 above 0.85 and MAPE below 12%. Ahmadianfar et al. [12] tested three data-driven techniques—locally weighted linear regression (LWLR), support vector regression (SVR), and multivariate linear regression (MLR)—to predict scour depth near vertical piles under wave action in sandy beds. LWLR attained an R^2 of 0.939 with an RMSE value of 0.075. Dang et al. [13] enhanced artificial neural network (ANN) models for estimating equilibrium-stage scour depth around circular piers by integrating firefly algorithms (FAs) and PSO. These hybrid models outperformed empirical equations and the Levenberg–Marquardt (LM) algorithm. Oğ & Bor [14] analyzed data from over 40 studies and applied hierarchical clustering and genetic programming (GP) to derive formulas through iterative optimization, achieving R^2 scores above 0.8 and improved generalization over existing empirical methods. Abd El-Hady Rady [15] combined GP with ANFIS to estimate local scour depth using 320 data points. Compared with ANFIS and regression-based models, GP demonstrated better accuracy. Recent studies have further expanded scour prediction research through the use of hybrid and ensemble machine learning techniques, including optimized XGBoost models, explainable artificial intelligence frameworks, and comparative assessments of data-driven and conventional approaches [4, 16, 17, 18, 19]. These studies demonstrate the growing capability of machine learning methods to capture complex scour mechanisms and improve predictive performance across a wide range of hydraulic and sediment conditions. Recent scour-depth studies have increasingly adopted hybrid, ensemble, and interpretable machine learning approaches. However, a unified benchmark comparison of KNN, RF, ANN, and SVM using the same clear-water circular-pier database, common input variables, consistent evaluation metrics, and identical empirical benchmarks remains relatively limited in the existing literature. The present study addresses this gap by providing a systematic comparison of these four machine learning algorithms under a common modeling framework.

The contribution of the present study lies in providing a systematic comparison of four widely used machine learning algorithms (KNN, ANN, RF, and SVM) using a unified database of clear-water scour observations collected from multiple experimental studies. In addition to model performance evaluation, the study investigates parameter sensitivity and benchmarks the ML models against established empirical scour equations. This provides a consistent framework for assessing the relative strengths and limitations of different prediction approaches under comparable conditions and contributes to the ongoing development of reliable data-driven tools for bridge scour assessment.

2. Methodology

2.1 Data Sources and Analysis

This study utilized data compiled from 23 previously published experimental studies. In total, 544 datasets representing clear-water scouring conditions (U/Uc < 1) around circular bridge piers were gathered, as summarized in Table 1. The compiled studies cover a wide range of hydraulic and sediment conditions, with individual study contributions ranging from 1 to 113 data points, thereby ensuring diversity and representativeness within the compiled database.

The scour depth influencing parameters, including approach flow depth (y), approach flow velocity (U), critical velocity (Uc), pier width (b), median grain size (d_{50}), and geometric standard deviation of bed material (σg), were used to predict scour depth around circular piers [20, 21]:

$$d_s = f\ (b, y, U, Uc, d_{50}, \sigma_g) \tag{1}$$

To reduce inconsistencies among collected datasets, minimize scaling effects, and improve model generalization capability under varying hydraulic and sediment conditions, all variables were converted into dimensionless forms. The transformed relationship can be expressed as [22, 23]:

$$\frac{ds}{y} = f\ \left(\frac{b}{y}, \frac{d50}{y}, \frac{U}{Uc}, Fr, \sigma_g\right) \tag{2}$$

where $Fr = U/\sqrt{gy}$ is the Froude number.

Five dimensionless input parameters were used: the pier width-to-flow depth ratio (b/y), the ratio of median sediment diameter to flow depth (d_{50}/y), the ratio of flow velocity to critical velocity (U/Uc), Froude number (Fr), and the geometric standard deviation of bed material (σg). The selected input parameters were chosen based on their well-established physical relevance to local scour processes and their widespread use in previous scour prediction studies [4, 9, 24, 25]. These variables collectively represent the key hydraulic (Fr, U/Uc), geometric (b/y), and sediment-related (d_{50}/y, σg) factors governing scour development around bridge piers. In addition, all selected parameters were consistently available across the compiled experimental database, ensuring a scientifically consistent basis for model development and comparison. The geometric standard deviation ranged from 1.15 to 3.7, indicating that the compiled datasets included both relatively uniform sediments (σg ≤ 1.5) and non-uniform sediments (σg > 1.5). The inclusion of σg as an input parameter allows the developed ML models to account for sediment gradation effects, including possible armouring behavior under non-uniform sediment conditions.

The dataset was randomly divided into training (85%, n = 461) and testing (15%, n = 83) subsets, as summarized in Table 2. During model development, the training subset was further partitioned using an internal hold-out strategy (80/20 split) for model tuning and selection of the optimal model configuration. In machine learning applications, validation and testing serve distinct purposes: the validation subset was used during model development to optimize model performance and reduce overfitting, whereas the independent testing subset was reserved exclusively for final unbiased performance evaluation of the developed models. This clear partitioning strategy ensures model robustness, generalization capability, reproducibility, and reliable assessment of predictive performance.

Descriptive statistics of the training and testing datasets, including maximum, minimum, mean, and standard deviation (SD) values of all dimensionless input parameters, are presented in Table 2. The close agreement between the statistical properties of the training and testing subsets indicates that the adopted random partitioning strategy preserved the overall data variability without introducing significant sampling bias.

Table 1 *Sources of experimental data used in this study*

Study	Number of Data Points
Chabert and Engeldinger [26]	72
Chee [27]	1
Melville [25]	9
Aksoy et al. [28]	28
Aksoy and Eski [29]	16

Study	Number of Data Points
Dey et al. [24]	4
Ettema [30]	13
Ettema [31]	38
Ettema et al. [32]	5
Graf [33]	3
Qaderi et al. [34]	113
Jain and Fischer [35]	2
Johnson and Torrico [36]	16
Lança et al. [37]	27
López et al. [38]	29
Laursen et al. [39]	7
Melville and Chiew [40]	27
Pandey et al. [41]	73
Shen et al. [42]	2
Sheppard and Miller [43]	2
Sheppard [44]	2
Wilson [45]	22
Yanmaz and Altinbilek [46]	33

Table 2 *Statistical indices of the training and testing datasets*

Parameters	Training datasets				Testing datasets			
	Max	Min	Mean	SD	Max	Min	Mean	SD
b/y	1.5	0.125	0.592	0.286	1.385	0.114	0.564	0.284
U/U_c	0.987	0.202	0.748	0.174	0.989	0.257	0.776	0.166
d_{50}/y	0.07	0.00105	0.015	0.016	0.07	0.00105	0.014	0.015
Fr	0.729	0.103	0.295	0.148	0.673	0.105	0.296	0.147
σ_g	3.7	1.15	1.522	0.523	3.7	1.15	1.562	0.521

2.2 Machine Learning Approaches

Local scour around bridge piers is governed by highly complex and nonlinear interactions among hydraulic, sediment, and geometric parameters [47]. These processes involve coupled effects such as flow separation, horseshoe vortex formation, sediment transport, and wake-induced sediment entrainment, all of which exhibit strong nonlinearity. Conventional linear regression and empirical approaches often fail to accurately capture these complex relationships, particularly across wide ranges of flow intensity, sediment gradation, and pier geometry. Therefore, nonlinear machine learning models (ANN, SVM, RF, and KNN) were adopted in this study, as they are capable of learning complex input–output relationships directly from data without requiring explicit assumptions regarding the functional form of the underlying processes. This capability enables improved representation of scour mechanisms and enhances predictive accuracy under diverse experimental conditions [16]. Detailed descriptions of the selected models are provided in the following subsections.

2.2.1 Artificial Neural Network (ANN)

An ANN is a well-known computational method inspired by the complex functionality of the human brain's neural system. It is a nonlinear modeling technique used to establish relationships between input variables and corresponding output data [48]. The ANN structure consists of input and output nodes separated by one or more hidden layers, with the interconnections referred to as weights (**Fig. 1**). Initially assigned random values, these weights are adjusted during training according to the difference between predicted and actual results. Activation functions in ANNs allow the network to manage nonlinearities and control neuron weights. Furthermore, the

Int. Journal of Integrated Engineering Vol. 18 No. 4 (2026) p. 217-237

training algorithm has a crucial influence on optimizing network accuracy by fine-tuning weights based on the training dataset to minimize prediction errors.

In the modeling process, the training dataset was first used for network learning, followed by the validation dataset to assess predictive capability. The final ANN configuration was determined after multiple iterations, ensuring satisfactory performance on validation data. A separate test dataset was then used to confirm model effectiveness.

In this study, a multilayer feedforward network (FNN) employing the Levenberg–Marquardt optimization method was implemented in MATLAB to identify the best-performing ANN configuration. The number of hidden layers and neurons per layer was selected through trial-and-error, adjusting hidden layer counts from 1 to 5 and neuron numbers from 5 to 20. A tangent sigmoid function was used for activation between the input and hidden layers, while a linear function was applied between the hidden layer and the output layer. The highest performance was achieved with a configuration of three hidden layers, each containing eight neurons.

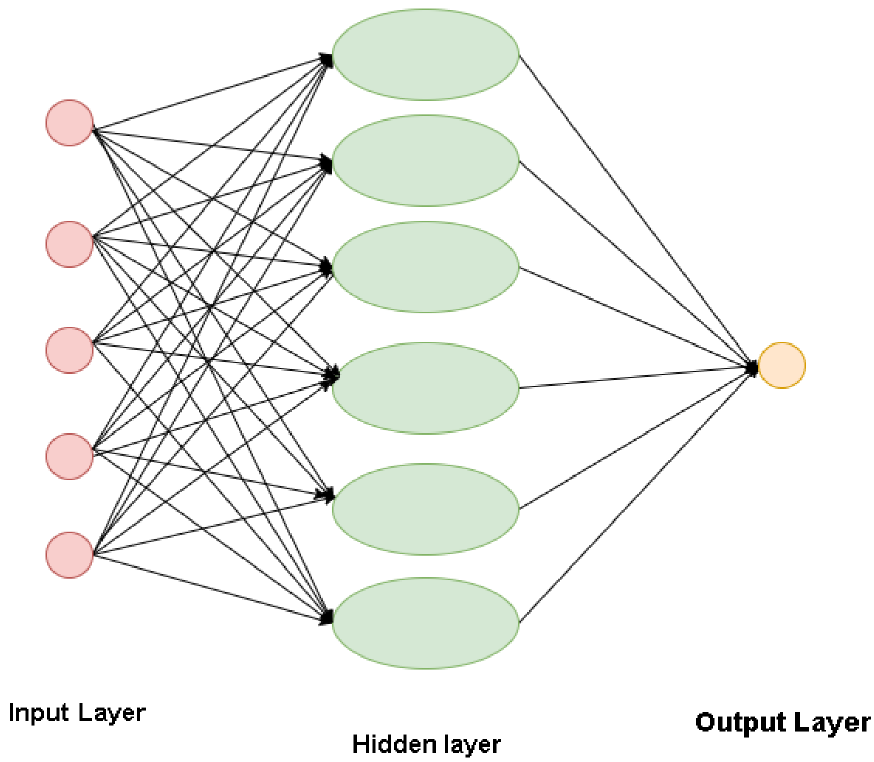

Fig. 1 *A schematic representation of an ANN [48]*

2.2.2 Support Vector Machine (SVM)

SVM, a robust machine-learning algorithm, was introduced by Vapnik in 1999 [49]. It serves as both a classification and regression tool for linear as well as nonlinear problems. SVMs enhance predictive performance by autonomously handling data while avoiding overfitting, adhering to the structural risk minimization (SRM) principle, and using convex optimization methods to reduce both empirical risk and confidence bounds simultaneously.

To address nonlinear problems, SVMs make use of kernel functions, applying the 'kernel trick' to transform data into higher-dimensional feature spaces where linear separation is achievable. Popular kernels, such as the Gaussian radial basis function (RBF), allow SVMs to capture complex patterns and classify datasets that are not linearly separable. In regression tasks, as adopted in this study, SVM is implemented as Support Vector Regression (SVR). In SVR, the margin hyperplane concept is adapted into an ε-insensitive tube surrounding the fitted regression plane rather than separating classes. The model seeks the flattest possible regression function while tolerating prediction errors within this predefined margin, thereby controlling model complexity and improving generalization capability for continuous scour depth prediction. Critical aspects of SVM design include choosing the right kernel type and determining whether to apply hard or soft margins. The SVM framework comprises selecting separating hyperplanes, defining kernel functions, and deciding on margin configurations (Fig. 2).

In this research, the SVM model was implemented in MATLAB (V.23) to estimate scour depth at a circular pier. The process began with the training dataset used for model learning, followed by validation data to assess predictive accuracy. The final SVM configuration was chosen after multiple iterations. Model performance was then verified using an independent test dataset.

The SVM model was tested using linear, polynomial, and radial basis function (RBF) kernels. The RBF kernel produced the most accurate scour depth estimates. Model accuracy was found to be highly sensitive to the tuning of parameters—namely, the penalty parameter (C), the RBF kernel width (gamma, g), and the epsilon-insensitive loss parameter (e). The optimal values for these parameters were determined iteratively, exploring C values between 1 and 500, g between 0.1 and 10, and e between 0.01 and 1. The best-performing setup used C = 10, g = 0.31, and e = 0.11 with the RBF kernel.

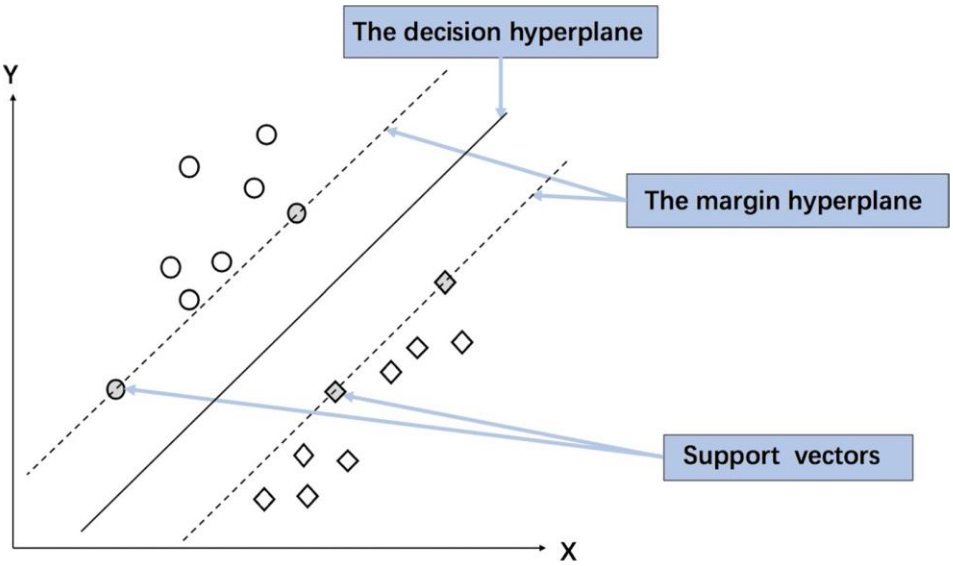

Fig. 2 *A schematic diagram of SVM learning [49]*

2.2.3 Random Forest (RF)

RF, a widely used machine-learning method introduced by Cutler and Breiman, integrates the outputs of multiple decision trees to produce a single prediction, making it effective for both classification and regression problems [50]. It is recognized for its high accuracy, resilience to noise, and ability to handle large, high-dimensional datasets. The approach uses structured decision trees in which branches indicate possible test results, internal nodes perform attribute evaluations, and leaf nodes provide either class labels or continuous values depending on the task. RF works by recursively splitting datasets according to the most relevant attributes, aiming to minimize impurity measures like Gini impurity or mean squared error. Its strength lies in processing complex datasets while reducing overfitting. Following the bagging concept, RF builds an ensemble of trees by training on random subsets (bootstrap samples) of the original data. Each tree generates its own prediction, and results are combined using majority voting for classification or averaging for regression, with the final outcome determined from these aggregated results.

In this work, RF regression is applied within the MATLAB environment using the ‘treebagger’ regression function to estimate scour depth. Model performance is influenced by tuning key parameters. These tunable parameters include the number of trees, maximum allowable splits, minimum leaf size, and others (**Fig. 3**).

The best parameter set is identified through iterative testing. Initially, the model is fitted on the training data and validated using the validation set by computing the root mean square error (RMSE). Different parameter combinations are examined, varying the number of trees from 10 to 200, the maximum number of splits from 10 to 280, and the minimum leaf size from 1 to 10.

Following this search process, the optimal settings are determined to be 58 trees, a minimum leaf size of 1, and a maximum split limit of 223. The optimal parameter combination was selected based on validation performance rather than training accuracy alone. In addition, the ensemble structure of RF, which combines predictions from multiple bootstrap-sampled decision trees, helps reduce model variance and mitigates the risk of severe overfitting. Finally, the model’s predictive capability is assessed on the test dataset using statistical evaluation metrics.

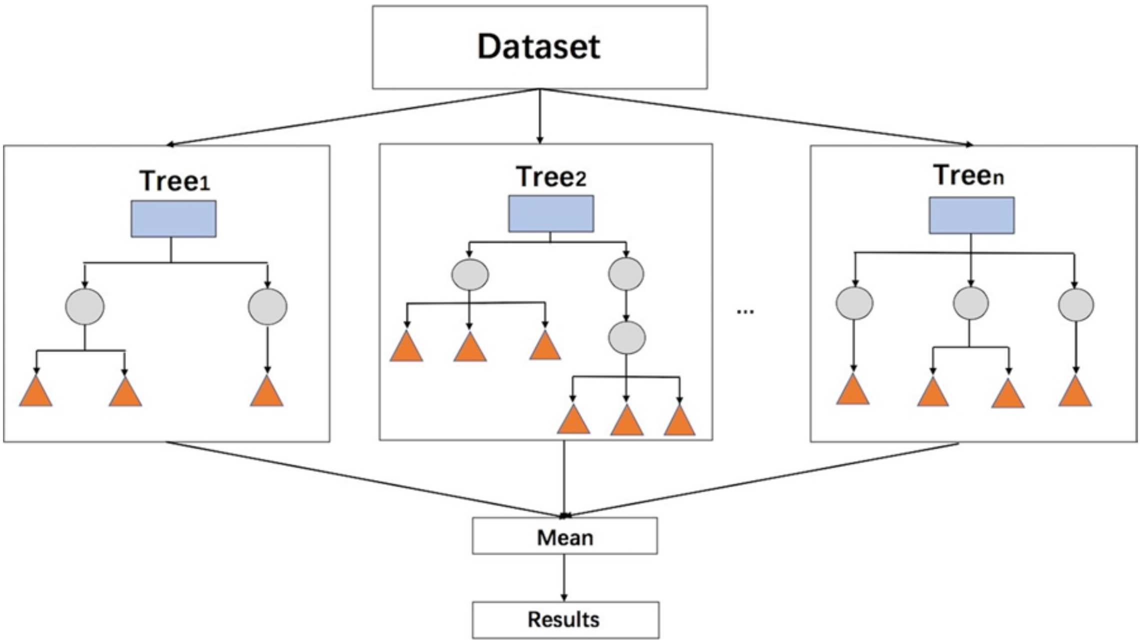

Fig. 3 *A schematic diagram of a random forest [51]*

2.2.4 K-Nearest Neighbors (KNNs)

KNN is a commonly applied supervised learning algorithm due to its straightforward design and strong performance in both classification and regression problems [52]. It is based on the premise that data points with comparable features are located close to each other within the feature space. For classification tasks, KNN assigns the new observation to the class most frequently appearing among its K nearest neighbors, while for regression, it estimates the output as the average of the target values from the K nearest points. Factors influencing KNN performance include the choice of K, the metric for measuring distances, neighbor weighting strategy, nearest-neighbor search method, and preprocessing approaches such as normalization.

Choosing an appropriate K value is essential; a very small K may lead to overfitting, while a very large K can result in underfitting. The prediction procedure involves computing distances from the query point to all other points, identifying the K closest, and then making predictions via majority voting (classification) or averaging (regression). Although KNN is conceptually simple, its computational cost increases with large datasets; therefore, optimized search structures like KD-trees or ball trees are often used to improve efficiency.

In this research, KNN is implemented in MATLAB, with performance mainly determined by two hyperparameters: the number of neighbors and the chosen distance measure. These parameters are tuned iteratively, testing K values from 1 to 20 and evaluating multiple distance measures (Fig. 4). The training set is first used to fit the model, followed by validation on a separate set where root mean square error (RMSE) is computed. Iterations continue until the lowest RMSE is achieved. The best configuration is identified as K = 1 with the 'cityblock' distance metric, using the smallest break-ties rule and exhaustive search. Although smaller K values may increase the risk of overfitting, K = 1 yielded the lowest validation RMSE among all tested configurations and was therefore selected as the optimal model based on validation performance. A final KNN model is then built with these settings, and its predictive ability is evaluated on the test dataset.

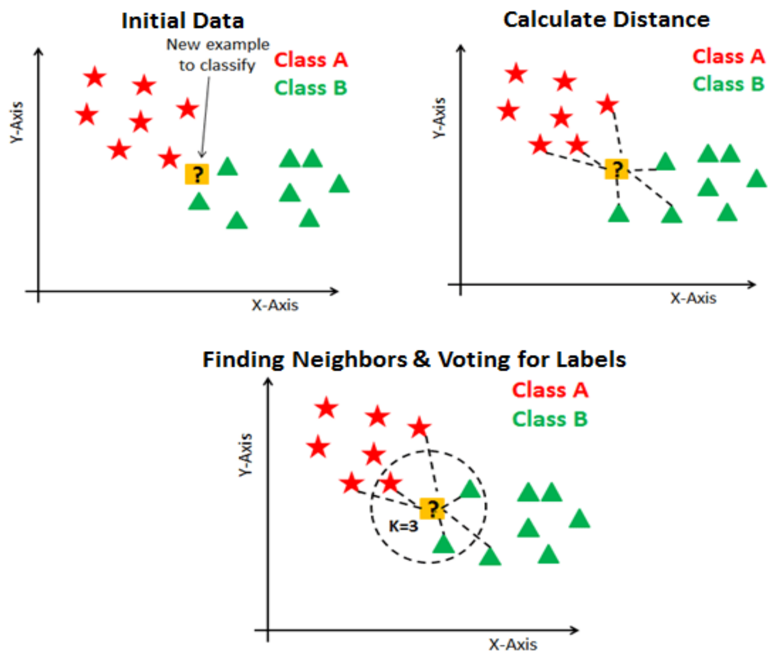

Fig. 4 *A schematic picture of KNN [45]*

2.3 Conventional Equations for Scour Depth

Although numerous empirical equations for scour depth prediction are available in the literature, only selected conventional equations were considered in this study based on the following criteria: (i) their widespread application and validation in previous bridge scour studies and engineering practice [25, 53], (ii) their applicability to clear-water scour conditions around circular bridge piers, which is consistent with the scope of the present study, and (iii) their incorporation of key hydraulic, geometric, and sediment-related parameters influencing local scour depth. In addition, these equations are structurally compatible with the variables available in the compiled experimental dataset, thereby ensuring a scientifically consistent and representative comparison with the developed machine learning models. The selected equations therefore provide reliable benchmark models for evaluating the predictive performance of the proposed ML approaches.

The CSU equation developed at Colorado State University, Jain and Fischer, Kim, and Ettema proposed empirical relationships to estimate the scour depth ratio (ds/y) around bridge piers on the basis of various hydraulic and geometric parameters. These equations, presented below as Eqs. (3) to (6), utilize parameters such as pier width (b), flow depth (y), the Froude number (Fr), and median sediment size (d_{50}).

The CSU equation [54] is one of the most widely used equations for estimating the equilibrium scour depth under clear-water conditions and incorporates pier shape, flow angle, and sediment factors:

$$\frac{ds}{y} = 2.0K_1\, K_2\, K_3\, K4\ \left(\frac{b}{y}\right)^{0.65} Fr^{0.43} \tag{3}$$

where K1 is the correction factor for the pier nose shape, K2 is the angle of attack, and K3 is the bed condition. The Jain and Fischer equation [35] considers the effect of the Froude number along with the pier width and flow depth:

$$\frac{ds}{y} = 1.84\, \left(\frac{b}{y}\right)^{0.7} Frc^{0.25} \tag{4}$$

The Kim equation [55] was developed via experimental data and incorporates sediment gradation:

$$\frac{ds}{y} = 0.69\, \left(\frac{b}{y}\right)^{0.35} \left(\frac{d50}{y}\right)^{-0.10} \sigma^{0.39}\, Fr^{0.56} \tag{5}$$

The Ettema equation [56] specifically focuses on clear-water scour and includes the Froude number (Fr):

$$\frac{ds}{y} = \left(\frac{b}{y}\right)^{0.38} Fr^{0.2} \left(\frac{b}{d50}\right)^{0.8} \tag{6}$$

Int. Journal of Integrated Engineering Vol. 18 No. 4 (2026) p. 217-237

2.4 Performance Analysis

In this study, the accuracy of the developed ML models is assessed using several statistical measures, including root mean square error (RMSE), mean absolute error (MAE), correlation coefficient (R^2), and Nash–Sutcliffe efficiency (NSE), as expressed below [20, 21, 57]:

$$\text{RMSE} = \sqrt{\frac{\sum_{i=1}^{N}(Xi-Yi)^2}{N}} \tag{7}$$

$$\text{MAE} = \frac{\sum_{i=1}^{N}|Xi-Yi|}{N} \tag{8}$$

$$R^2 = \frac{\sum_{i=1}^{N}(Xi-\bar{X})(Yi-\bar{Y})}{\sqrt{\sum_{i=1}^{N}(Xi-\bar{X})^2 . \sum_{i=1}^{N}(Yi-\bar{Y})^2}} \tag{9}$$

$$\text{NSE} = 1- (\frac{\sum_{i=1}^{N}(Xi-Yi)^2}{\sum_{i=1}^{N}(Xi-\bar{X})^2}) \tag{10}$$

where Xi denotes the observed value for the ith data point, Yi is the corresponding predicted value, $\bar{X}$ is the average of the observed dataset, $\bar{Y}$ is the average of the predicted dataset, and N indicates the total number of observations.

3. Results and Discussion

3.1 Performance of the ML Models

The model performances assessed using the statistical metrics RMSE, MAE, R^2, and NSE for both training and testing datasets are summarized in Table 3. Comparison of these metrics indicates that in the training stage, the KNN and RF models outperformed the other two models, showing smaller RMSE and MAE values along with higher R^2 and NSE scores. Likewise, in the testing phase, KNN and RF models exhibited better predictive capability than ANN and SVM. The KNN and RF models exhibited higher performance during training than testing, with KNN achieving an R^2 of 0.9978 during training and 0.894 during testing, while RF achieved an R^2 of 0.9836 during training and 0.888 during testing. The observed reduction in performance from training to testing may indicate some degree of overfitting, which is expected in data-driven models when evaluated on unseen data. Nevertheless, both models maintained strong predictive performance on the independent testing dataset, indicating satisfactory generalization capability. Furthermore, the RF model inherently incorporates overfitting control through bootstrap aggregation and random feature selection, while the KNN model configuration was selected based on validation performance, where K = 1 yielded the lowest validation RMSE among the tested configurations.

Table 3 *Statistical indices for the training and testing phases of the ML models*

Model name	Dataset	Phase	RMSE	MAE	R^2	NSE
KNN	378	Training	0.0188	0.0025	0.9978	0.9978
	83	Testing	0.1158	0.0943	0.894	0.891
ANN	378	Training	0.121	0.0828	0.913	0.913
	83	Testing	0.1273	0.0918	0.87	0.87
SVM	378	Training	0.1107	0.0834	0.9244	0.9242
	83	Testing	0.1228	0.0899	0.8812	0.8783
RF	378	Training	0.0582	0.0421	0.9836	0.979
	83	Testing	0.1179	0.0904	0.888	0.8878

The scatter plots for training and testing datasets corresponding to the ANN, SVM, KNN, and RF models are presented in Figs. 5–8. During training, the models capture the relationships between input variables, as reflected by R^2 values ranging from 0.913 to 0.997, with the majority of points falling within a 20% error margin. Among the models, KNN and RF achieved higher R^2 values compared with ANN and SVM.

In the testing phase, the models also deliver satisfactory predictions, with R^2 values between 0.870 and 0.894, and most predicted points remain within a 20% deviation range, as seen in Figs. 5–8. The scatter plots demonstrate that predicted values are closely aligned with the regression line, with the majority of points within a 20% error range, indicating strong predictive performance of the models.

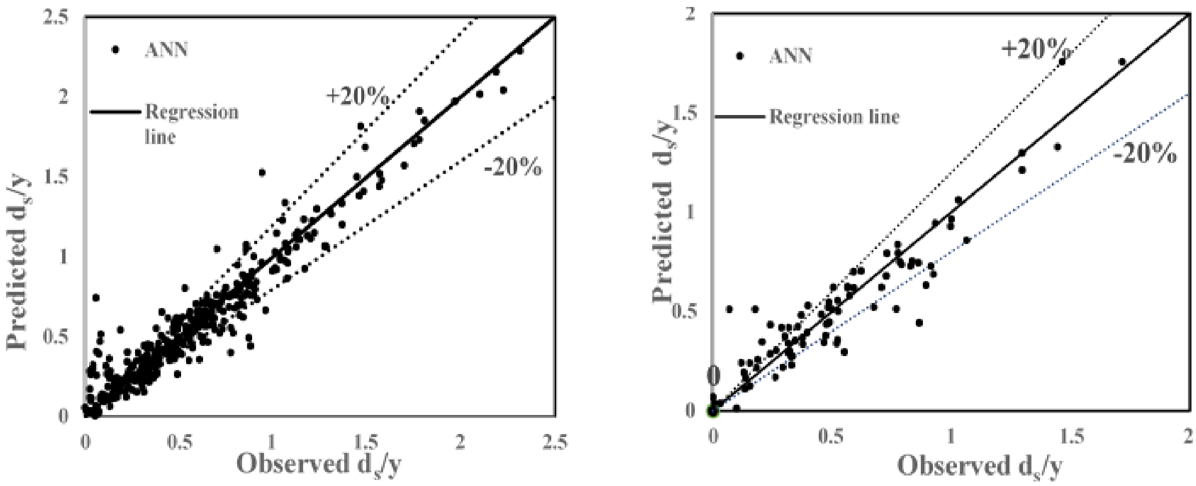

(a) (b)

Fig. 5 *Scatter plot of the ANN model during the (a) Training; and (b) Testing phases*

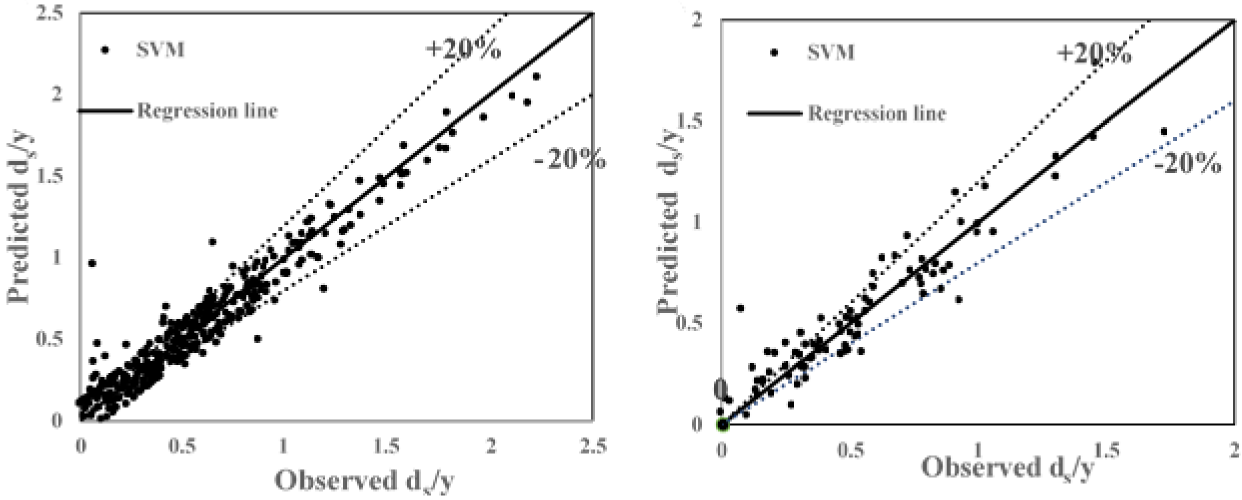

(a) (b)

Fig. 6 *Scatter plot of the SVM model during the (a) Training; and (b) Testing phases*

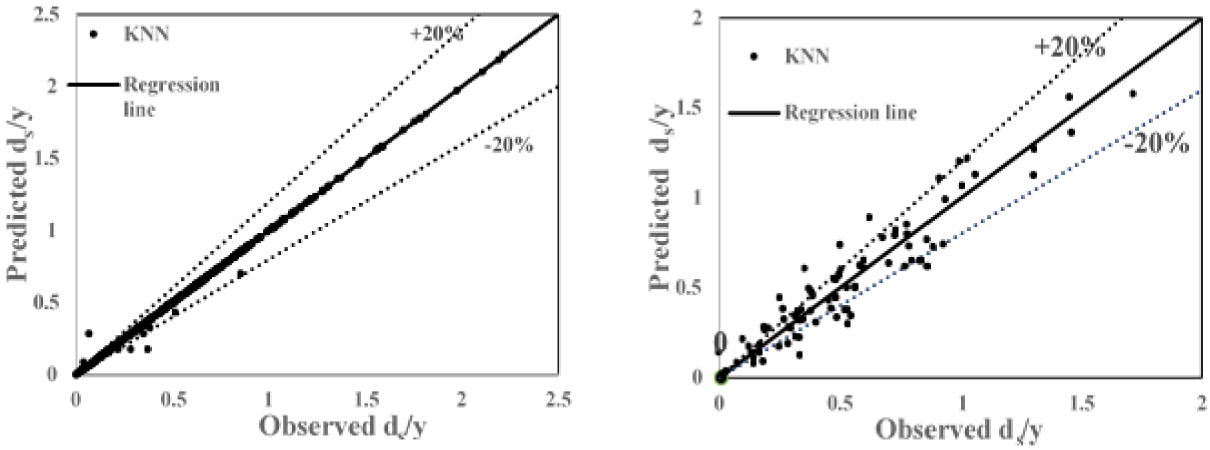

(a) (b)

Fig. 7 *Scatter plot of the KNN model during the (a) Training; and (b) Testing phases*

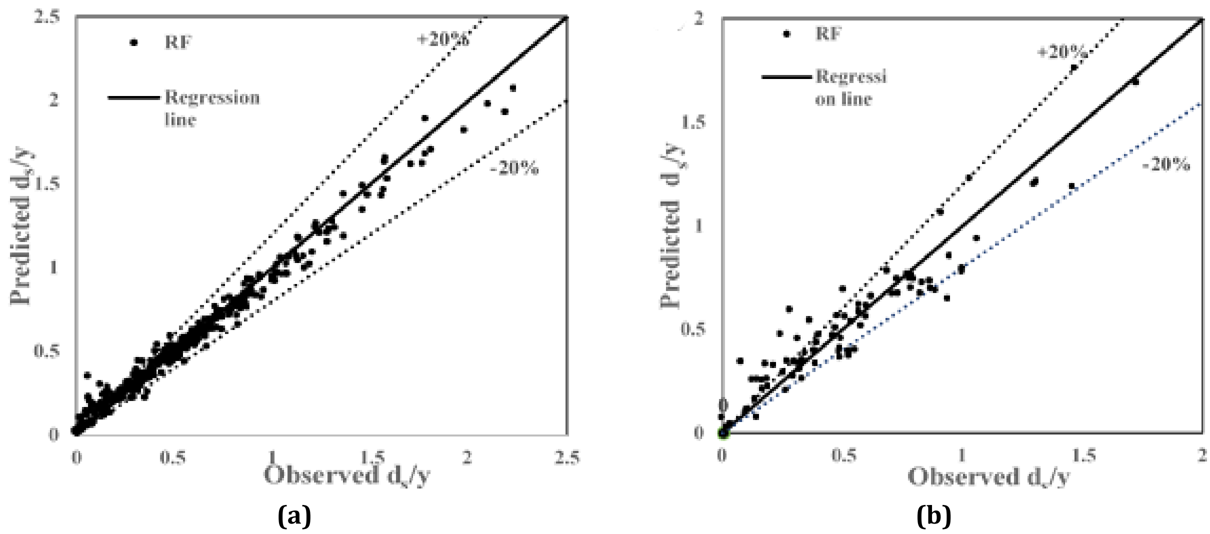

Fig. 8 *Scatter plot of the RF model during the (a) Training; and (b) Testing phases*

For further evaluation, box and violin plots are presented in Figs. 10 and 11, respectively. In the box plot, the box represents the central 50% of the dataset, showing the median line and mean value, while the whiskers extend to points within 1.5 times the interquartile range. The plot indicates that all model predictions follow a distribution pattern similar to the observed data, suggesting that the models effectively capture the central tendency of the data. Among the models, the KNN model demonstrates the closest match to the observed distribution, as reflected in the box positions.

The violin plot in Fig. 11 offers a more detailed view of the distribution patterns for both observed and predicted data. Unlike box plots, violin plots provide additional information by combining a kernel density estimate with traditional box plot elements. The violin resembles a box plot with a central box but expands outward on both sides to represent the spread of data points. The width of the violin reflects data density across different value ranges, revealing the underlying shape of the distribution. Wider sections near the median indicate a higher concentration of values, whereas narrow ends reflect lower density. The violin plot demonstrates that all models generally reproduce medians and interquartile ranges comparable to the observed data. Moreover, the overall shapes of the violin plots for the models closely match the observed distribution. Among the models, the SVM model exhibits the shape most similar to the observed data.

To achieve a more comprehensive assessment of the effectiveness of the proposed methods, a Taylor diagram is utilized in Fig. 12 to examine the agreement between observed and predicted values. The Taylor diagram provides a useful way to summarize multiple evaluation metrics in a single, informative visualization. It simultaneously displays key statistical indicators such as standard deviation (SD), the correlation between observed and predicted values, and the centered RMSE. Analysis of the Taylor diagram shows that the ANN, SVM, and RF models tend to slightly underestimate scour depth relative to the observed data (denoted by the red reference line). In contrast, the KNN model predictions align more closely with the measured values. Furthermore, the diagram indicates a strong correlation between observed and predicted values across all models. Overall, the KNN model demonstrates superior performance compared with the other approaches.

3.2 Comparison Between the ML Models and Empirical Equations

In this study, empirical equations were also applied to estimate scour depth. Table 4 presents the statistical metrics for both the ML model predictions and the results obtained from the empirical equations. Comparison of these metrics shows that the ML models consistently deliver better performance than the empirical approaches, as indicated by the superior statistical values achieved by the ML predictions. The higher NSE values (ranging from 0.87 to 0.891) of the ML models demonstrate their enhanced predictive capability compared with the conventional methods. In contrast, the negative NSE values obtained for the CSU and Jain and Fischer equations indicate that these empirical models performed worse than using the mean observed scour depth as a predictor. This highlights the limited applicability of these formulations to the compiled dataset and further demonstrates the superior predictive capability of the ML models. This indicates that the ML models have a higher ability to accurately forecast scour depth than traditional empirical equations.

Table 4 *Statistical indices of the ML models and empirical equations*

	Models	Type of data	Number of data	RMSE	MAE	R^2	NSE
Machine learning models	KNN	Test	83	0.1158	0.0943	0.894	0.891
	ANN	Test	83	0.1273	0.0918	0.87	0.87
	SVM	Test	83	0.1228	0.0899	0.8812	0.8783
	RF	Test	83	0.1179	0.0904	0.888	0.8878
Empirical equations	CSU	Test	83	0.508	0.364	0.217	-1.087
	Kim	Test	83	0.346	0.286	0.083	0.035
	Ettema	Test	83	0.419	0.343	0.312	-0.415
	Jain and Fischer	Test	83	0.557	0.415	0.207	-1.509

The scatter plot in Fig. 9 illustrates the relationship between predicted and observed values for both the ML models and empirical equations. The plot demonstrates that ML predictions are more closely aligned with observed values than the conventional methods. In particular, ML model predictions adhere closely to the regression line, with R^2 values ranging from 0.87 to 0.894, and most predicted points fall within the 20% error margin. In contrast, predictions from the empirical equations show greater deviations from the regression line. Specifically, empirical predictions, especially those from the CSU and Jain & Fischer equations, often overestimate the observed values and frequently fall outside the 20% error range.

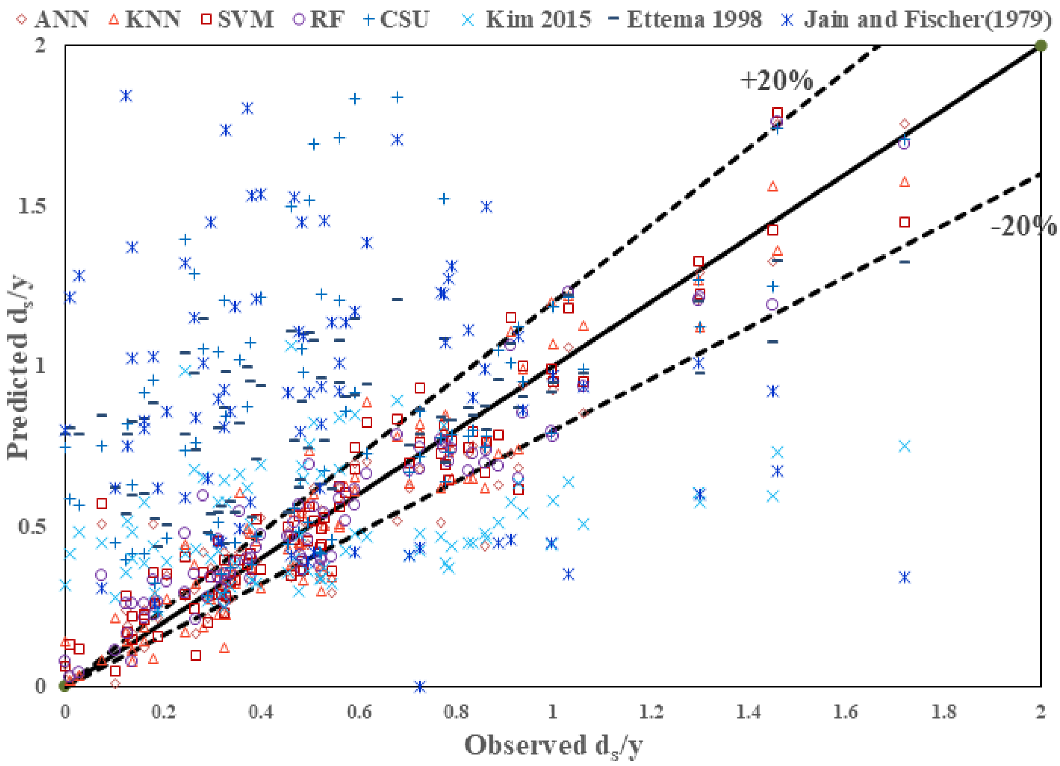

Fig. 9 *Scatter plot of the ML models and empirical equations*

The analysis presented in Figs. 10 and 11 offers a detailed comparison between ML model predictions and empirical equation outputs in reproducing the distributional characteristics of the observed scour depth data. In Fig. 10, the box plots show that the ML models closely match the observed distribution, with comparable median values, interquartile ranges (IQRs), and overall spread. The similarity in box positions and whisker lengths indicates that the ML models successfully reproduce both the central tendency and variability of the observed data. In contrast, the empirical equations generally exhibit higher median values and wider distributions, particularly the CSU (median: 0.79) and Jain and Fischer equations (median: 0.92), suggesting a tendency toward overprediction and greater dispersion. The larger IQRs and extended whiskers observed for these equations indicate higher variability and reduced consistency relative to the observed data.

The violin plots in Fig. 11 further illustrate the distributional behavior of the predictions. The ML models produce violin shapes that closely resemble the observed distribution, indicating comparable density concentration (0.3–0.7 ds/y) and spread across the range of normalized scour depths. Conversely, the empirical equations exhibit distributions shifted toward higher scour depth values, reflecting positive skewness and a tendency to overestimate scour depth. The broader upper tails observed for the CSU, Ettema, and Jain and Fischer equations indicate larger dispersion and greater sensitivity to high scour depth predictions. Furthermore, the density distributions of the ML models remain concentrated within the same range as the observed data, whereas the empirical equations display noticeable shifts in distributional shape and spread (density concentration varies 0.3-1.2). Overall, the ML models demonstrate better agreement with the observed distribution in terms of central tendency, spread, and distributional shape, whereas the empirical equations show greater skewness and variability.

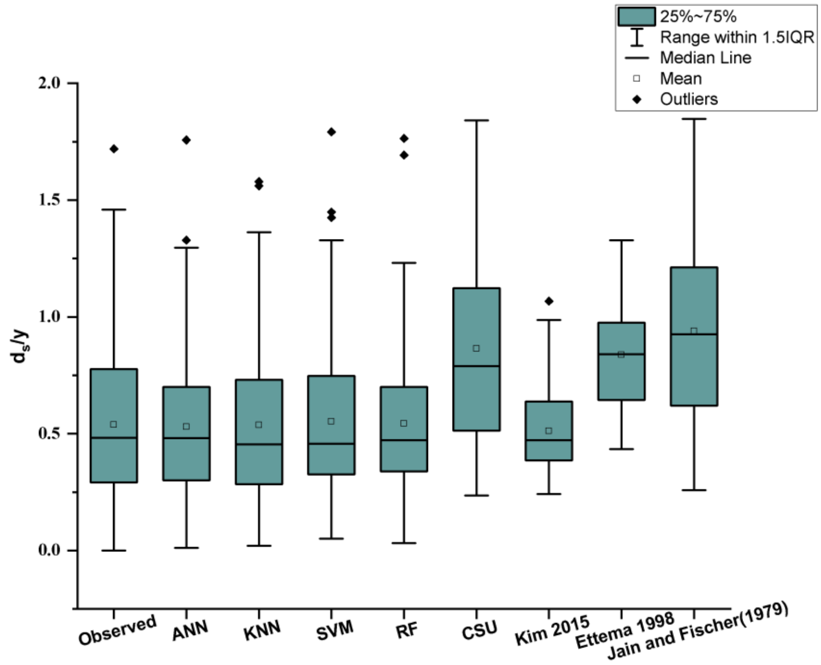

Fig. 10 *Box plots of the ML models and empirical equations*

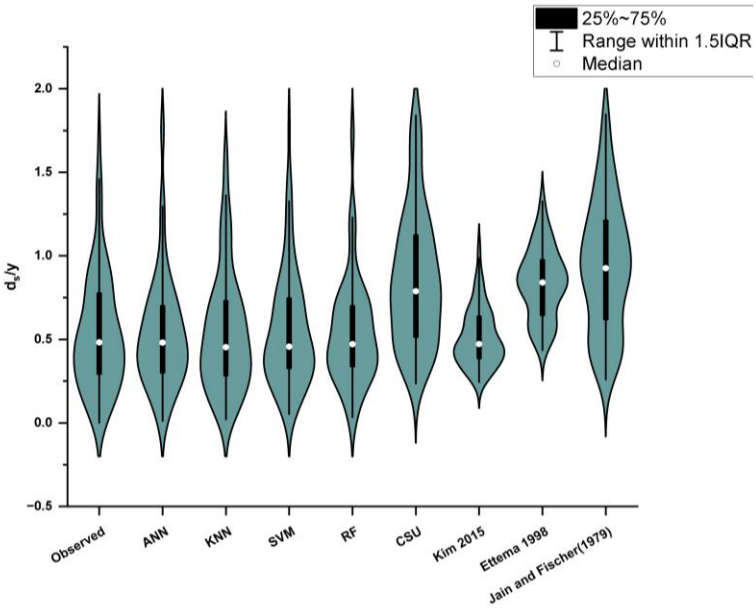

Fig. 11 *Violin plot of the ML models and empirical equations*

The Taylor diagram in Fig. 12 highlights a distinct difference between the two prediction approaches. The ML model predictions exhibit standard deviations that are closely aligned with the reference line, indicating strong consistency with the measured scour depth values. Furthermore, the correlation coefficient for the ML models, ranging from 0.9 to 0.95, demonstrates a robust linear association with the observed values. The closeness of the ML predictions to the red reference point in the diagram further confirms a high level of agreement between predicted and actual data. In contrast, the conventional equation results show a clear deviation from the reference line in the Taylor diagram, reflecting lower effectiveness compared with the ML models in capturing the underlying trends in the data. The correlation coefficients for these empirical equations, ranging from 0.2 to 0.6, indicate a weaker linear relationship with the observed measurements. Overall, the Taylor diagram emphasizes the superior accuracy of ML models over conventional formulas, demonstrating their capability to reliably predict scour depths while preserving strong linear correlation with observed values.

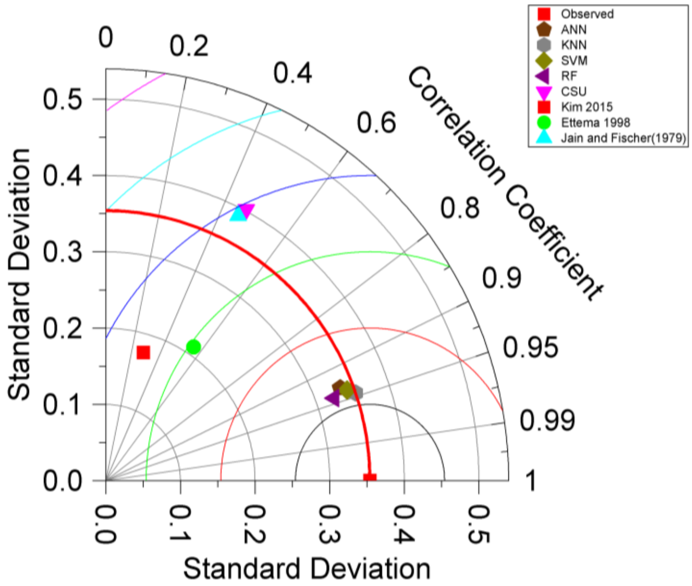

Fig. 12 *Taylor diagram of the ML models and empirical equations*

3.3 Sensitivity Analysis

A sensitivity analysis was performed for the KNN, ANN, RF, and SVM models to identify the most critical dimensionless parameter for predicting local scour depth. In this procedure, each of the five input parameters was removed individually to evaluate its influence on the model output. The results for the ML models under each condition are summarized in Table 5. The findings reveal that the dimensionless parameter b/y exerts the strongest effect on predicting normalized scour depth, as evidenced by its lower R^2 and NSE values and higher RMSE and MAE values. In contrast, d_{50}/y has the least influence on the prediction of normalized scour depth. To provide a clearer ranking and normalized measure of parameter importance, the average reduction in testing R^2 across all four models was calculated after removing each input parameter. These reductions were subsequently normalized to sum to 100%, yielding a relative importance score for each variable. The results are summarized in Table 6. The normalized ranking indicates that the pier width-to-flow depth ratio (b/y) is the most influential parameter, accounting for 50.5% of the total predictive importance, followed by sediment gradation (σg, 28.8%), flow intensity (U/Uc, 11.1%), Froude number (Fr, 6.0%), and sediment size ratio (d50/y, 3.6%). This analysis quantitatively reinforces the dominant role of geometric and hydraulic factors in local scour prediction.

Table 5 *Sensitivity analysis of different models*

Input Parameters	Model Name	Training				Testing			
		RMSE	MAE	R^2	NSE	RMSE	MAE	R^2	NSE
b/y, U/U_c, Fr, σ_g	ANN	0.143	0.0943	0.8785	0.8783	0.1711	0.128	0.7798	0.7636
	SVM	0.1114	0.0837	0.9234	0.9232	0.1229	0.0902	0.8808	0.878
	KNN	0.0188	0.0025	0.9978	0.9978	0.1158	0.0943	0.894	0.891
	RF	0.0526	0.0381	0.9856	0.9829	0.1298	0.0926	0.8659	0.8639
b/y, U/U_c, d_{50}/y, σ_g	ANN	0.1208	0.0815	0.9131	0.9131	0.1462	0.1125	0.829	0.827
	SVM	0.1477	0.1083	0.8661	0.865	0.1754	0.1292	0.7713	0.7513
	KNN	0.0188	0.0025	0.9978	0.9978	0.1379	0.1069	0.8582	0.8465
	RF	0.0544	0.0393	0.9851	0.9817	0.1193	0.0878	0.8857	0.885
b/y, U/U_c, d_{50}/y, Fr	ANN	0.1722	0.1251	0.8241	0.8234	0.1984	0.1494	0.69	0.6823
	SVM	0.1683	0.1256	0.825	0.8247	0.2345	0.165	0.6028	0.5562
	KNN	0.0188	0.0025	0.9978	0.9978	0.252	0.1595	0.6063	0.486
	RF	0.0694	0.0494	0.9764	0.9702	0.1836	0.1246	0.7321	0.7279
U/U_c, d_{50}/y, Fr, σ_g	ANN	0.3506	0.2553	0.2889	0.2683	0.3003	0.2383	0.2716	0.2704
	SVM	0.2682	0.1861	0.5684	0.5547	0.2619	0.1842	0.4479	0.4461
	KNN	0.0188	0.0025	0.9978	0.9978	0.2513	0.1889	0.58	0.49
	RF	0.1442	0.0977	0.8774	0.8713	0.2146	0.1549	0.6505	0.628
b/y, d_{50}/y, Fr, σ_g	ANN	0.1776	0.1233	0.8141	0.8123	0.1682	0.1162	0.7832	0.7715
	SVM	0.1854	0.1296	0.7882	0.7872	0.1838	0.1241	0.7404	0.7272
	KNN	0.0188	0.0025	0.9978	0.9978	0.1627	0.1169	0.811	0.786
	RF	0.0682	0.0469	0.9762	0.9712	0.1356	0.1017	0.8531	0.8616

Table 6 *Normalized relative importance and ranking of input parameters based on sensitivity analysis*

Parameter Removed	Average Reduction in Testing R^2	Normalized Relative Importance (%)	Rank
b/y	0.3958	50.5	1
σg	0.2255	28.8	2
U/Uc	0.0864	11.1	3
Fr	0.0473	6.04	4
d_{50}/y	0.0282	3.60	5

Note: The normalized relative importance (Ii%) = ($\Delta Ri^2/\sum_{j=1}^{n} \Delta Rj^2$) ×100, where n = total number of input parameters.

The sensitivity analysis results can also be interpreted within the framework of established scour mechanisms. The dominant influence of the pier width-to-flow depth ratio (b/y) is consistent with the critical role of pier geometry in controlling flow contraction, downflow intensity, and the formation of horseshoe vortices around the pier base, which are the primary drivers of local scour development [58, 59]. Similarly, the importance of flow intensity (U/Uc) and Froude number (Fr) reflects the influence of hydraulic forces and sediment transport processes on scour initiation and evolution. The contribution of sediment gradation (σg) can be associated with armouring effects and particle mobility, whereas the relatively lower influence of d_{50}/y is physically reasonable because grain-size effects are already partially represented through the velocity ratio (U/Uc). Overall, the parameter importance ranking (b/y > σg > U/Uc > Fr > d_{50}/y) is consistent with established scour mechanics, indicating that the ML models capture physically meaningful relationships rather than merely statistical correlations.

3.4 Comparison with Existing Studies

A critical comparison of the reported results indicates that differences in model accuracy among studies are strongly influenced by dataset characteristics, model architecture, input parameter selection, and validation procedures. Studies reporting exceptionally high predictive accuracy often employ larger datasets, numerical simulation data, homogeneous experimental conditions, or hybrid and optimized machine learning frameworks such as ANN–PSO and RPSO–XGBoost. In contrast, the present study utilized a diverse multi-source laboratory database compiled from 23 independent experimental studies under clear-water scour conditions. Such diversity introduces greater variability in hydraulic, sediment, and measurement conditions, making the prediction task inherently more challenging while improving the generalization capability of the developed models. Therefore, direct comparison of statistical metrics across studies should be interpreted with caution, and **Table 7** should be viewed as a qualitative benchmark rather than a direct quantitative ranking of model performance. Despite differences in predictive accuracy, the findings consistently indicate the superior performance of ML models over conventional empirical equations and highlight the importance of geometric parameters in scour depth prediction.

Table 7 *Comparison of the results with those of previous studies*

Author	Data type	Number of data points	Models used	Best model	RMSE and R^2 of the best model	Comparison with conventional equation	Most influential Parameter (sensitivity analysis)
Qaderi et al. [34]	Laboratory	Total-148 Training-130 Testing-30	GMDH, SVM, ANFIS, ANN, GEP	ANFIS	0.038 and 0.971	Yes	-
Shalini & Roshni [60]	Laboratory & Field	Total-213 Training-160 Testing-53	GEP, ANFIS, MARS, M5-TREE	ANFIS	0.062 and 0.986	Yes	-
Siahkali et al. [53]	Laboratory	Total-246 Training-172 Validation-37 Testing-37	ANNs, Kriging, MARS, GMDH	Kriging	0.065 and 0.947	Yes	Pier diameter
Ahmadianfar et al. [12]	Laboratory	Total-111 Training-83 Testing-28	LWLR, SVR, MLR	LWLR	0.075 and 0.939	Yes	Keulegan–Carpenter number
Hassan et al. [61]	Numerical simulation by FLOW 3D	Total-729 Training-692 Testing-37	ANN, GEP, NLR	ANN	0.029 and 0.969	No	Flow depth
Fuladipanah et al. [17]	Laboratory & Field	Total-455 Training-319 Testing-136	SVM, GEP, MLP, GBT, MARS	SVM	0.023 and 0.984	Yes	-
Dang et al. [13]	Laboratory	Total-192 Training-132 Validation-30 Testing-30	ANN-PSO, ANN-FA, ANN-LM	ANN-PSO	12.622 and 0.979	No	-

Author	Data type	Number of data points	Models used	Best model	RMSE and R^2 of the best model	Comparison with conventional equation	Most influential Parameter (sensitivity analysis)
Hassan & Jalal [10]	Numerical simulation by FLOW-3D	Total-243 Training-195 Testing-48	GEP, NLR	GEP	0.142 and 0.901	No	Depth of flow
Eini et al. [9]	Laboratory	Total-841 Training-589 Validation-126 Testing-126	XGBoost, PSO – XGBoost, RFO – XGBoost, RPSO – XGBoost	RPSO – XGBoost	0.0398 and 0.928	Yes	Pier diameter
Bateni et al. [62]	Laboratory	Total-347 Training-243 Testing-104	GEP and MARS	MARS	0.0220 and 0.902	Yes	Pile diameter
This study	Laboratory	Total-544 Training-463 Testing-81	ANN, SVM, KNN, RF	KNN	0.1158 and 0.894	Yes	Pier width

4. Conclusion

In this study, the KNN, ANN, RF, and SVM models were applied to estimate local scour depth around circular piers, with their results compared against traditional empirical approaches. The key conclusions are as follows:

1. The machine learning (ML) models provided satisfactory predictions within the tested range of dimensionless parameters.
2. Among the models, KNN and RF achieved the lowest RMSE along with the highest R^2 and NSE values, demonstrating strong predictive capability.
3. SVM and RF exhibited the lowest MAEs, suggesting greater accuracy in minimizing absolute prediction errors.
4. Overall, the KNN model outperformed the other models while being computationally efficient.
5. All the ML models surpassed existing empirical equations in scour depth forecasting.
6. A sensitivity analysis revealed that the pier width–to–flow depth ratio (b/y) was the most influential factor in predicting normalized scour depth, whereas the sediment size–to–flow depth ratio (d_{50}/y) had the least influence.

These results hold practical significance for bridge foundation design, where precise prediction of scour depth enables safer and more cost-effective mitigation measures. The developed ML models offer a robust alternative to conventional empirical methods, particularly in cases where traditional equations underperform.

However, certain limitations remain in this study. While the models proved resilient against the inherent variability of multi-source laboratory data, they were developed under clear-water conditions and may not generalize to live-bed scenarios. Their applicability is also restricted to single circular piers, and performance could decline for other pier shapes or configurations. As data-driven tools, these models require sufficient high-quality training datasets and may underperform in field conditions that differ significantly from the training data. In addition, the developed models were trained exclusively on laboratory datasets and therefore may not fully capture the complexities associated with field-scale applications, including flow unsteadiness, sediment heterogeneity, debris accumulation, and site-specific hydraulic conditions. The predictive performance of the models may also vary when applied to live-bed scour conditions or bridge foundations with complex geometries, multiple piers, or pier groups, which were not considered in the present study. Future work should expand model applicability to various pier geometries, pier groups, live-bed scour conditions, and additional hydraulic parameters. Incorporating more diverse laboratory and field datasets would further enhance model robustness, generalization capability, and real-world reliability. Moreover, future studies should consider a broader range of empirical scour equations, such as the Nandi and Das equation, the Sheppard and Miller equation, and the Melville and Coleman integrated framework, together with advanced and hybrid machine learning approaches (e.g., ANFIS/GEP, ANN–PSO, SVM-based models, M5-tree, and XAI/XGBoost-based frameworks) for more comprehensive comparative evaluation. In addition, alternative neighborhood sizes (K values) and more extensive validation strategies, such as k-fold cross-validation, should be investigated to further improve the generalization capability of KNN-based scour prediction models. Future studies should also incorporate uncertainty quantification, statistical significance analysis, and advanced explainable artificial intelligence techniques, such as SHAP values, permutation importance analysis, and feature attribution methods, to provide a more rigorous evaluation of prediction reliability and parameter importance.

Acknowledgement

The authors would like to extend their sincere appreciation to the Department of Water Resources Engineering, Chittagong University of Engineering and Technology, along with the distinguished instructors and support personnel (Arpan Paul & Mohammad Shaifullah), for their important mentorship throughout the work.

Conflict of Interest

The authors declare that they have no conflicts of interest.

Author Contribution

The authors confirm contribution to the paper as follows: ***study conception and design****: Md. Ashraful Islam, Md. Mukdiul Islam;* ***data collection****: Md. Mukdiul Islam;* ***analysis and interpretation of results****: Md. Ashraful Islam, Md. Mukdiul Islam, Md. Bashirul Islam;* ***draft manuscript preparation****: Md. Samiun Basir, Md. Bashirul Islam. All authors reviewed the results and approved the final version of the manuscript.*

References

[1] M. Al-Jubouri, R. P. Ray, and E. H. Abbas, "Advanced Numerical Simulation of Scour around Bridge Piers: Effects of Pier Geometry and Debris on Scour Depth," *J. Mar. Sci. Eng.*, vol. 12, no. 9, Art. no. 9, Sep. 2024, doi: 10.3390/jmse12091637.

[2] J. V. Klinga and A. Alipour, "Assessment of structural integrity of bridges under extreme scour conditions," *Eng. Struct.*, vol. 82, pp. 55–71, Jan. 2015, doi: 10.1016/j.engstruct.2014.07.021.

[3] M. Sasidharan, A. K. Parlikad, and J. Schooling, "Risk-informed asset management to tackle scouring on bridges across transport networks," *Struct. Infrastruct. Eng.*, vol. 18, no. 9, pp. 1300–1316, Sep. 2022, doi: 10.1080/15732479.2021.1899249.

[4] A. Choudhary, B. S. Das, K. Devi, and J. R. Khuntia, "ANFIS- and GEP-based model for prediction of scour depth around bridge pier in clear-water scouring and live-bed scouring conditions," *J. Hydroinformatics*, vol. 25, no. 3, pp. 1004–1028, May 2023, doi: 10.2166/hydro.2023.212.

[5] A. Harasti, G. Gilja, N. Adžaga, and M. Žic, "Analysis of Variables Influencing Scour on Large Sand-Bed Rivers Conducted Using Field Data," *Appl. Sci.*, vol. 13, no. 9, Art. no. 9, Jan. 2023, doi: 10.3390/app13095365.

[6] S. Kumar, G. Oliveto, V. Deshpande, M. Agarwal, and U. Rathnayake, "Forecasting of time-dependent scour depth based on bagging and boosting machine learning approaches," *J. Hydroinformatics*, vol. 26, no. 8, pp. 1906–1928, Jul. 2024, doi: 10.2166/hydro.2024.047.

[7] Z. U. Khan *et al.*, "Advanced Prediction Models for Scouring Around Bridge Abutments: A Comparative Study of Empirical and AI Techniques," *Water*, vol. 16, no. 21, Art. no. 21, Jan. 2024, doi: 10.3390/w16213082.

[8] S. M. Bateni, S. M. Borghei, and D. S. Jeng, "Neural network and neuro-fuzzy assessments for scour depth around bridge piers," *Eng. Appl. Artif. Intell.*, vol. 20, no. 3, pp. 401–414, Apr. 2007, doi: 10.1016/j.engappai.2006.06.012.

[9] N. Eini, S. M. Bateni, C. Jun, E. Heggy, and S. S. Band, "Estimation and interpretation of equilibrium scour depth around circular bridge piers by using optimized XGBoost and SHAP," *Eng. Appl. Comput. Fluid Mech.*, vol. 17, no. 1, 2023, doi: 10.1080/19942060.2023.2244558.

[10] W. H. Hassan and H. K. Jalal, "Prediction of the depth of local scouring at a bridge pier using a gene expression programming method," *SN Appl. Sci.*, vol. 3, no. 2, Feb. 2021, doi: 10.1007/s42452-020-04124-9.

[11] V. Kumar, A. Baranwal, and B. S. Das, “Prediction of local scour depth around bridge piers: modelling based on machine learning approaches,” *Eng. Res. Express*, vol. 6, no. 1, Mar. 2024, doi: 10.1088/2631-8695/ad08ff.

[12] I. Ahmadianfar, M. Jamei, and X. Chu, “Prediction of local scour around circular piles under waves using a novel artificial intelligence approach,” *Mar. Georesources Geotechnol.*, vol. 39, no. 1, pp. 44–55, 2021, doi: 10.1080/1064119X.2019.1676335.

[13] N. M. Dang, D. Tran Anh, and T. D. Dang, “ANN optimized by PSO and Firefly algorithms for predicting scour depths around bridge piers,” *Eng. Comput.*, vol. 37, no. 1, pp. 293–303, 2021, doi: 10.1007/s00366-019-00824-y.

[14] K. Oğuz and A. Bor, “Prediction of Local Scour around Bridge Piers Using Hierarchical Clustering and Adaptive Genetic Programming,” *Appl. Artif. Intell.*, vol. 36, no. 1, 2022, doi: 10.1080/08839514.2021.2001734.

[15] R. Abd El-Hady Rady, “Prediction of local scour around bridge piers: artificial-intelligence-based modeling versus conventional regression methods,” *Appl. Water Sci.*, vol. 10, no. 2, Feb. 2020, doi: 10.1007/s13201-020-1140-4.

[16] N. Murtaza, D. Khan, A. Rezzoug, Z. U. Khan, B. Benzougagh, and K. M. Khedher, “Scour depth prediction around bridge abutments: A comprehensive review of artificial intelligence and hybrid models,” *Phys. Fluids*, vol. 37, no. 2, p. 021306, Feb. 2025, doi: 10.1063/5.0244974.

[17] M. Fuladipanah, M. A. Hazi, and O. Kisi, “An in-depth comparative analysis of data-driven and classic regression models for scour depth prediction around cylindrical bridge piers,” *Appl. Water Sci.*, vol. 13, no. 12, pp. 1–22, 2023, doi: 10.1007/s13201-023-02022-0.

[18] B. Nandi, G. Patel, and S. Das, “Prediction of maximum scour depth at clear water conditions: Multivariate and robust comparative analysis between empirical equations and machine learning approaches using extensive reference metadata,” *J. Environ. Manage.*, vol. 354, p. 120349, Mar. 2024, doi: 10.1016/j.jenvman.2024.120349.

[19] B. Nandi, G. Patel, and S. Das, “Machine learning prediction of flow-induced scour depth around isolated pier comparing stand-alone and ensemble models,” *Eng. Appl. Artif. Intell.*, vol. 156, p. 111318, Sep. 2025, doi: 10.1016/j.engappai.2025.111318.

[20] A. Baranwal, P. Gaurav, L. Reddy, B. S. Das, and B. Naik, “Predicting temporal clear water scour depth around bridge piers with XGBoost and SVM–PSO approaches,” *J. Hydroinformatics*, vol. 26, no. 12, pp. 3109–3129, Nov. 2024, doi: 10.2166/hydro.2024.119.

[21] B. Nandi and S. Das, “Identify most promising temporal scour depth formula for circular piers proposed over last six decades,” *Ocean Eng.*, vol. 286, p. 115639, Oct. 2023, doi: 10.1016/j.oceaneng.2023.115639.

[22] A. Kumar, A. Baranwal, and B. S. Das, “Modelling of clear water scour depth around bridge piers using M5 tree and ANN-PSO,” *AQUA - Water Infrastruct. Ecosyst. Soc.*, vol. 72, no. 8, pp. 1386–1403, Aug. 2023, doi: 10.2166/aqua.2023.225.

[23] Nil, A. Baranwal, and B. S. Das, “Clear-water and live-bed scour depth modelling around bridge pier using support vector machine,” *Can. J. Civ. Eng.*, vol. 50, no. 6, pp. 445–463, Jun. 2023, doi: 10.1139/cjce-2022-0237.

[24] S. Dey, S. K. Bose, and G. L. N. Sastry, “Clear Water Scour at Circular Piers: a Model,” *J. Hydraul. Eng.*, vol. 121, no. 12, pp. 869–876, 1995, doi: 10.1061/(asce)0733-9429(1995)121:12(869).

[25] B. W. Melville, “Pier and Abutment Scour: Integrated Approach,” *J. Hydraul. Eng.*, vol. 123, no. 2, pp. 125–136, Feb. 1997, doi: 10.1061/(ASCE)0733-9429(1997)123:2(125).

[26] J. Chabert and E. P., *Etude des affouillements autour des piles de ponts*. France: Laboratoire National d’Hydraulique, Chatou, 1956. [Online]. Available: https://search.worldcat.org/pt/title/etude-des-affouillements-autour-des-piles-de-ponts/oclc/216784257

[27] R. K. W. Chee, “Live-bed scour at bridge piers,” School of Engineering, University of Auckland, Auckland, New Zealand, 290, 1982.

[28] A. O. Aksoy, G. Bombar, T. Arkis, and M. S. Guney, “Study of the time-dependent clear water scour around circular bridge piers,” *J. Hydrol. Hydromech.*, vol. 65, no. 1, pp. 26–34, Dec. 2016, doi: 10.1515/johh-2016-0048.

[29] A. O. Aksoy and O. Y. Eski, “Experimental investigation of local scour around circular bridge piers under steady state flow conditions,” *J. South Afr. Inst. Civ. Eng.*, vol. 58, no. 3, pp. 21–27, Sep. 2016, doi: 10.17159/2309-8775/2016/v58n3a3.

[30] R. Ettema, “Influence of bed material gradation on local scour,” Dept. of Civ. Engrg., University of Auckland, Auckland, New Zealand, M.S. Thesis 124, 1976.

[31] R. Ettema, “Scour at bridge piers,” Dept. of Civ. Engrg., University of Auckland, Auckland, New Zealand, PhD Thesis 216, 1980.

[32] R. Ettema, G. Kirkil, and M. Muste, “Similitude of Large-Scale Turbulence in Experiments on Local Scour at Cylinders,” *J. Hydraul. Eng.*, vol. 132, no. 1, pp. 33–40, Jan. 2006, doi: 10.1061/(ASCE)0733-9429(2006)132:1(33).

[33] W. H. Graf, “Load scour around piers,” Laboratoire de Recherches Hydrauliques, Ecole Polytechnique Federale de Lausanne, Lausanne, Switzerland, 1995.

[34] K. Qaderi, F. Javadi, M. R. Madadi, and M. M. Ahmadi, “A comparative study of solo and hybrid data driven models for predicting bridge pier scour depth,” *Mar. Georesources Geotechnol.*, vol. 39, no. 5, pp. 589–599, 2021, doi: 10.1080/1064119X.2020.1735589.

[35] S. C. Jain and E. E. Fischer, “Scour Around Circular Bridge Piers at High Froude Numbers.,” Iowa Univ., Iowa City. Inst. of Hydraulic Research.; Federal Highway Administration, Washington, DC., Springfield, Virginia, PB80139322, 1979. Accessed: Jan. 06, 2025. [Online]. Available: https://ntrl.ntis.gov/NTRL/dashboard/searchResults/titleDetail/PB80139322.xhtml

[36] P. A. Johnson and E. F. Torrico, “Scour around wide piers in shallow water,” *Transp. Res. Rec.*, no. 1471, pp. 66–70, Dec. 1994.

[37] R. M. Lança, C. S. Fael, R. J. Maia, J. P. Pêgo, and A. H. Cardoso, “Clear-Water Scour at Comparatively Large Cylindrical Piers,” *J. Hydraul. Eng.*, vol. 139, no. 11, pp. 1117–1125, 2013, doi: 10.1061/(asce)hy.1943-7900.0000788.

[38] G. López, L. Teixeira, M. Ortega-Sánchez, and G. Simarro, “Estimating Final Scour Depth under Clear-Water Flood Waves,” *J. Hydraul. Eng.*, vol. 140, no. 3, pp. 328–332, 2014, doi: 10.1061/(asce)hy.1943-7900.0000804.

[39] E. M. Laursen, E. V. Richardson, J. R. Richardson, and B. W. Melville, “Discussions and Closure: Pier and Abutment Scour: Integrated Approach,” *J. Hydraul. Eng.*, vol. 124, no. 7, pp. 769–774, 1998, doi: 10.1061/(asce)0733-9429(1998)124:7(769).

[40] B. W. Melville and Y.-M. Chiew, “Time Scale for Local Scour at Bridge Piers,” *J. Hydraul. Eng.*, vol. 125, no. 1, pp. 59–65, Jan. 1999, doi: 10.1061/(ASCE)0733-9429(1999)125:1(59).

[41] M. Pandey, G. Oliveto, J. H. Pu, P. K. Sharma, and C. S. P. Ojha, “Pier scour prediction in non-uniform gravel beds,” *Water Switz.*, vol. 12, no. 6, pp. 13–17, 2020, doi: 10.3390/W12061696.

[42] H. W. Shen, V. R. Schneider, and S. Karaki, “Local Scour Around Bridge Piers,” *J. Hydraul. Div.*, vol. 95, no. 6, pp. 1919–1940, Nov. 1969, doi: 10.1061/JYCEAJ.0002197.

[43] D. M. Sheppard and W. Miller, “Live-Bed Local Pier Scour Experiments,” *J. Hydraul. Eng.*, vol. 132, no. 7, pp. 635–642, Jul. 2006, doi: 10.1061/(ASCE)0733-9429(2006)132:7(635).

[44] D. M. Sheppard, “Overlooked local sediment scour mechanism,” *Transp. Res. Rec.*, no. 1890, pp. 107–111, 2004, doi: 10.3141/1890-13.

[45] K. V. Wilson, “Scour at selected bridge sites in Mississippi,” US Department of the Interior, US Geological Survey, Reston, Virginia, Resources Investigation Report 94–4241, 1995.

[46] A. M. Yanmaz and H. D. Altinbilek, “Study of Time-Depenbent Local Scour around Bridge Piers,” *J. Hydraul. Eng.*, vol. 117, no. 10, pp. 1247–1268, Oct. 1991, doi: 10.1061/(ASCE)0733-9429(1991)117:10(1247).

[47] N.-D. Hoang, K.-W. Liao, and X.-L. Tran, “Estimation of scour depth at bridges with complex pier foundations using support vector regression integrated with feature selection,” *J. Civ. Struct. Health Monit.*, vol. 8, no. 3, pp. 431–442, Jul. 2018, doi: 10.1007/s13349-018-0287-2.

[48] M. M. Taye, “Understanding of Machine Learning with Deep Learning: Architectures, Workflow, Applications and Future Directions,” *Computers*, vol. 12, no. 5, Art. no. 5, May 2023, doi: 10.3390/computers12050091.

[49] N. Cristianini and E. Ricci, “Support Vector Machines,” in *Encyclopedia of Algorithms*, M.-Y. Kao, Ed., Boston, MA: Springer US, 2008, pp. 928–932. doi: 10.1007/978-0-387-30162-4_415.

[50] H. Tyralis, G. Papacharalampous, and A. Langousis, “A Brief Review of Random Forests for Water Scientists and Practitioners and Their Recent History in Water Resources,” *Water*, vol. 11, no. 5, Art. no. 5, May 2019, doi: 10.3390/w11050910.

[51] Z. M. Zou, D. H. Chang, H. Liu, and Y. D. Xiao, “Current updates in machine learning in the prediction of therapeutic outcome of hepatocellular carcinoma: what should we know?,” *Insights Imaging*, vol. 12, no. 1, 2021, doi: 10.1186/s13244-021-00977-9.

[52] E. Ozturk Kiyak, B. Ghasemkhani, and D. Birant, “High-Level K-Nearest Neighbors (HLKNN): A Supervised Machine Learning Model for Classification Analysis,” *Electronics*, vol. 12, no. 18, Art. no. 18, Jan. 2023, doi: 10.3390/electronics12183828.

[53] M. Z. Siahkali, A. Ghaderi, A. Bahrpeyma, and M. Rashki, “Estimating Pier Scour Depth : Comparison of Empirical Formulations,” vol. 9, no. 1, pp. 109–128, 2021, doi: 10.22044/jadm.2020.10085.2147.

[54] E. V. Richardson, S. Karaki, K. Mahmood, D. B. Simons, and M. A. Stevens, “Highways in the River Environment–Hydraulic and Environmental Design Considerations: Basic Course Instructor’s Lesson Plans,” Department of Transportation, Federal Highway Administration, United States, 1975. [Online]. Available: https://rosap.ntl.bts.gov/view/dot/75304/dot_75304_DS1.pdf

[55] I. Kim, M. Y. Fard, and A. Chattopadhyay, “Investigation of a Bridge Pier Scour Prediction Model for Safe Design and Inspection,” *J. Bridge Eng.*, vol. 20, no. 6, p. 04014088, Jun. 2015, doi: 10.1061/(ASCE)BE.1943-5592.0000677.

[56] R. Ettema, E. A. Mostafa, B. W. Melville, and A. A. Yassin, “Local Scour at Skewed Piers,” *J. Hydraul. Eng.*, vol. 124, no. 7, pp. 756–759, Jul. 1998, doi: 10.1061/(ASCE)0733-9429(1998)124:7(756).

[57] B. Nandi and S. Das, “Maximum scour depth estimation around side-by-side piers due to spacing effects for sustainable hydraulic infrastructure design,” *Sustain.*, vol. 5, p. 100134, Jan. 2025, doi: 10.1016/j.nxsust.2025.100134.

[58] R. kumar Behera, E. Padhi, and G. D. Singhal, “Recent trends in local scour countermeasure for bridge piers,” *Eng. Sci. Technol. Int. J.*, vol. 77, p. 102367, May 2026, doi: 10.1016/j.jestch.2026.102367.

[59] A. Baranwal and B. S. Das, “Scouring around bridge pier: A comprehensive analysis of scour depth predictive equations for clear-water and live-bed scouring conditions,” *AQUA - Water Infrastruct. Ecosyst. Soc.*, vol. 73, no. 3, pp. 424–452, Feb. 2024, doi: 10.2166/aqua.2024.235.

[60] S. Shalini and T. Roshni, “Application of GEP, M5-TREE, ANFIS, and MARS for Predicting Scour Depth in Live Bed Conditions around Bridge Piers,” *J. Soft Comput. Civ. Eng.*, vol. 7, no. 4, pp. 24–49, 2023, doi: 10.22115/scce.2023.369213.1559.

[61] W. H. Hassan, H. H. Hussein, M. H. Alshammari, H. K. Jalal, and S. E. Rasheed, “Evaluation of gene expression programming and artificial neural networks in PyTorch for the prediction of local scour depth around a bridge pier,” *Results Eng.*, vol. 13, Mar. 2022, doi: 10.1016/j.rineng.2022.100353.

[62] S. M. Bateni, H. R. Vosoughifar, B. Truce, and D. S. Jeng, “Estimation of Clear-Water Local Scour at Pile Groups Using Genetic Expression Programming and Multivariate Adaptive Regression Splines,” *J. Waterw. Port Coast. Ocean Eng.*, vol. 145, no. 1, p. 04018029, Jan. 2019, doi: 10.1061/(ASCE)WW.1943-5460.0000488.